Facile syntheses and electrocatalytic properties of porous Pd and its alloy nanospheres

ARTICLE *in* JOURNAL OF MATERIALS CHEMISTRY · APRIL 2011

Impact Factor: 7.44 · DOI: 10.1039/c0jm04407e

9 AUTHORS, INCLUDING:

Lei Zhang
Georgia Institute of Technology
21 PUBLICATIONS **470** CITATIONS
SEE PROFILE

Zhiyuan Jiang
Xiamen University
37 PUBLICATIONS **1,252** CITATIONS
SEE PROFILE

Shuifen Xie
Xiamen University
39 PUBLICATIONS **1,212** CITATIONS
SEE PROFILE

Qin Kuang
Xiamen University
80 PUBLICATIONS **3,894** CITATIONS
SEE PROFILE

Journal of Materials Chemistry

Dynamic Article Links

Cite this: *J. Mater. Chem.*, 2011, **21**, 9620

www.rsc.org/materials

PAPER

Facile syntheses and electrocatalytic properties of porous Pd and its alloy nanospheres

Lei Zhang, Jiawei Zhang, Zhiyuan Jiang,* Shuifen Xie, Mingshang Jin, Xiguang Han, Qin Kuang, Zhaoxiong Xie* and Lansun Zheng

Received 16th December 2010, Accepted 27th April 2011
DOI: 10.1039/c0jm04407e

Pd-based catalysts are of great interest both for fundamental research and applications. It still remains a challenge to develop reliable and versatile approaches to prepare Pd-based nanostructures with higher performance and better stability. In this article, a facile solution route has been developed to prepare Pd nanospheres, as well as Pd–Pt, Pd–Ag and Pd–Pt–Ag alloy nanospheres. SEM and TEM investigations revealed that the as-prepared nanospheres were three-dimensionally interconnected porous networks with primary nanoparticles as building blocks. The chemical composition of these nanospheres can be easily adjusted by controlling the molar ratio of precursors. Electrochemical measurements indicated that the electrocatalytic activity of these nanospheres towards formic acid oxidation depended on the composition of the nanospheres. By judiciously adjusting the composition of the Pd based alloy nanospheres, the performance of the Pd based catalysts, *i.e.*, the onset potential of the formic acid oxidation, the corresponding peak current density and the ability to tolerate CO, can be optimized.

Introduction

Fuel cells have attracted extensive interest in the past decades due to their high energy density, little or no pollution and the possibility of their use as an alternative energy source to power many electronic components.[1,2] Among various types of fuel cell, direct fuel cells using formic acid as the fuel have many advantages. For example, formic acid is nontoxic and common to the environment. Formic acid is expected to facilitate both electron and proton transport within the anode compartment of the fuel cell, and direct formic acid fuel cells (DFAFCs) have high electromotive force, limited fuel crossover, and reasonable power densities at low temperatures.[3–6] Pt is the most widely used catalyst in fuel cells.[7,8] However, besides the fact that Pt catalysts are readily poisoned by CO during the oxidation of fuel, the high cost of Pt and supply constraints limits its large-scale application in these types of fuel cells.[9,10] Many investigations were therefore focused on the exploration of reduced or non-platinum catalysts that can offer acceptable performance. Pd-based catalysts were considered as a substitute of platinum in fuel cells due to their attractive performance and better CO tolerance during formic acid oxidation than that of Pt catalysts.[9,11]

Recently, several strategies have been developed to improve the performance of Pd-based catalysts in DFAFCs. A general way is to increase the surface area of the Pd catalysts as the reactions only occur on the surface or interface of the catalyst. Directed by this strategy, hollow palladium nanospheres,[12,13] monodisperse palladium nanoparticles,[14] palladium nanowire networks,[15] nanoporous palladium,[16,17] one-dimensional flower-like palladium nanoparticles[18] and so on, have been synthesized in order to generate a large surface area. Another strategy for improving the activity and stability is to use Pd-based bimetallic structures or alloys instead of pure Pd as the catalyst. It has been reported that Pd–Pt bimetallic nanodendrites,[19–21] PdPt nanocubes,[22,23] titanium-supported bimetallic Pt-Pd/Ti networks,[24] three-dimensional Pt-on-Pd bimetallic nanodendrites on graphene nanosheets[25] may enhance the electro-oxidation activity in some kinds of fuel cells. The third way is to prepare micro-/nanocrystals with relatively high energy surfaces, which usually have high electrocatalytic activity.[26–28] Although many efforts have been devoted to improve the performance of the Pd-based catalysts used in the fuel cells, it remains a challenge to develop reliable and versatile approaches to prepare Pd-based nanostructures with higher performance and better stability.

Herein, aimed at increasing the surface area and alloying, a facile solution route has been developed to prepare porous Pd nanospheres, Pd–Pt, Pd–Ag, and Pd–Pt–Ag alloy nanospheres. The composition of these nanospheres can be easily adjusted. Electrochemical measurements indicated that the electrocatalytic activity of these alloy nanospheres towards formic acid oxidation depended on chemical composition of the Pd-based alloy nanospheres. The $Pd_3Pt_{0.5}Ag_{0.5}$ alloy nanospheres had much higher catalytic activity for formic acid electro-oxidation and better CO tolerance than other as-prepared nanospheres.

Key Laboratory for Physical Chemistry of Solid Surfaces & Department of Chemistry, College of Chemistry and Chemical Engineering, Xiamen University, Xiamen, 361005, China. E-mail: zyjiang@xmu.edu.cn; zxxie@xmu.edu.cn

Experimental

Materials

Sodium tetrachloropalladate(II) hydrate ($Na_2PdCl_4 \cdot 3H_2O$, 99.95%), dihydrogen hexachloroplatinate hexahydrate ($H_2PtCl_6 \cdot 6H_2O$, 99.95%) and sodium borohydride ($NaBH_4$, 97%) were used as received from Alfar Aesar. Silver nitrate ($AgNO_3$, analytical grade) and L-ascorbic acid (AA, analytical grade) were used as received from Sinopharm Chemical Reagent Co., Ltd. Cetyltrimethyl ammonium chloride (CTAC, analytical grade) was received from Tianjin Guangfu Fine Chemical Research Institute. All aqueous solutions were prepared with ultrapure water.

Synthesis of Pd seeds

An aqueous CTAC solution (10.0 ml, 0. 10 mol L^{-1}) was added into an aqueous Na_2PdCl_4 solution (0.050 ml, 0.050 mol L^{-1}) at room temperature. To this solution, a freshly prepared aqueous $NaBH_4$ solution (0.10 ml, 0.10 mol L^{-1}) was quickly added with a gentle shaking. The seeds were aged for 3 h to decompose the excess borohydride.

Synthesis of Pd nanospheres

An aqueous CTAC solution (5.0 ml, 0.010 mol L^{-1}) and 0.10 ml as-prepared Pd seeds were added into an aqueous Na_2PdCl_4 solution (3.0 ml, 1.0 mmol L^{-1}) at room temperature, and mixed by gentle shaking. Then a freshly prepared aqueous AA solution (0.10 ml, 0.10 mol L^{-1}) was quickly added with gentle shaking. The mixed solution was kept at room temperature for 10 min.

Synthesis of Pd–Pt nanospheres

To get porous Pd_3Pt_1 and $Pd_3Pt_{0.5}$ alloy nanospheres, a higher temperature was needed. An aqueous H_2PtCl_6 solution (1.0 ml or 0.5 ml, 1.0 mmol L^{-1}) was added into the growth solution (mixture of 5 ml 0.01 mol L^{-1} CTAC solution, 0.10 ml as-prepared Pd seed and 3.0 ml 1.0 mmol L^{-1} Na_2PdCl_4 solution) at room temperature before adding AA solution. Then the mixed solution was kept at a temperature of 70 °C for 10 min. The products were denoted as Pd_3Pt_1 or $Pd_3Pt_{0.5}$ nanospheres according to the molar ratio of the precursor, and similarly hereinafter.

Synthesis of Pd–Ag nanospheres

The synthesis was similar to that for preparing Pd nanospheres. An aqueous $AgNO_3$ solution (1.0 ml or 0.5 ml, 1.0 mmol L^{-1}) was added into the growth solution (mixture of 5.0 ml 0.01 mol L^{-1} CTAC solution and 3.0 ml 1.0 mmol L^{-1} Na_2PdCl_4 solution). The mixed solution was also kept at room temperature for 10 min after adding AA aqueous solution.

Synthesis of Pd–Pt–Ag nanospheres

An aqueous CTAC solution (5.0 ml, 0.010 mol L^{-1}), 0.10 ml the Pd seeds, an aqueous $AgNO_3$ solution (1.0 ml or 0.50 ml, 1.0 mmol L^{-1}) and an aqueous H_2PtCl_6 solution (1.0 ml or 0.50 ml, 1.0 mmol L^{-1}) was added into an aqueous Na_2PdCl_4 solution (3.0 ml, 1.0 mmol L^{-1}) at room temperature in turn. Then, a freshly prepared aqueous AA solution (0.10 ml, 0.10 mol L^{-1}) was quickly added to this solution with a gentle shaking. The mixed solution was kept in an oven at a temperature of 70 °C for 10 min.

Sample treatment

After the reaction, the samples were centrifuged at 10 000 rpm for 20 min and washed with ultrapure water twice.

Structural characterizations

The morphology and structure of the products were characterized by scanning electron microscopy (SEM, S-4800), transmission electron microscopy (TEM, JEM-2100) and X-ray powder diffraction (XRD, Panalytical X-pert diffractometer with Cu-Kα radiation).

Electrochemical measurements

A glassy carbon electrode (diameter of 5 mm) was carefully polished and washed before every experiment. Then, the as-prepared porous nanosphere suspensions were dripped onto the surface of the glassy carbon electrode and dried at room temperature. The cyclic voltammetry (CV) measurements were carried out using an electrochemical workstation (CHI 631a, Shanghai Chenhua Co. China). A Pt sheet and a standard calomel electrode (SCE) served as the counter and reference electrodes, respectively. All the electrode potentials in this paper are quoted *versus* the SCE.

Results and discussion

Characterization of the porous Pd and its alloy nanospheres

The morphologies of the products were investigated by the SEM, as shown in Fig. 1. It can be seen that the palladium sample consists of spherical particles with relatively uniform diameter of 33 ± 5 nm. Their surfaces were rough and detailed observation shows that the individual spheres are composed of irregular nanoparticles with a size of about 7 nm (insert of Fig. 1a). The morphologies of the Pd_3Ag_1 sample (Fig. 1b) were also spheroidal and their diameters were 36 ± 7 nm. These spheres were also assembled from smaller nanoparticles as the primary building blocks. Similarly, the Pd_3Pt_1 (Fig. 1c) and $Pd_3Pt_{0.5}Ag_{0.5}$ samples (Fig. 1d) have hierarchical structures with sizes of 25–40 nm.

The structural features of the nanospheres were further revealed by TEM, as shown in Fig. 2. It can be seen that the products were relatively uniform porous spheres. The size of the porous palladium nanospheres (Fig. 2a), Pd_3Ag_1 nanospheres (Fig. 2b), Pd_3Pt_1 nanospheres (Fig. 2c) and $Pd_3Pt_{0.5}Ag_{0.5}$ nanospheres (Fig. 2d) are in the range of 25–50 nm, which is consistent to the SEM observations. A careful survey of the TEM images reveals that each of the nanospheres were actually a three-dimensionally interconnected porous network with primary nanoparticles acting as building blocks. The Pd nanospheres consisted of nanorods with a diameter of about 3 nanometer and length in the range of 5–10 nm. The Pd_3Ag_1 nanospheres were

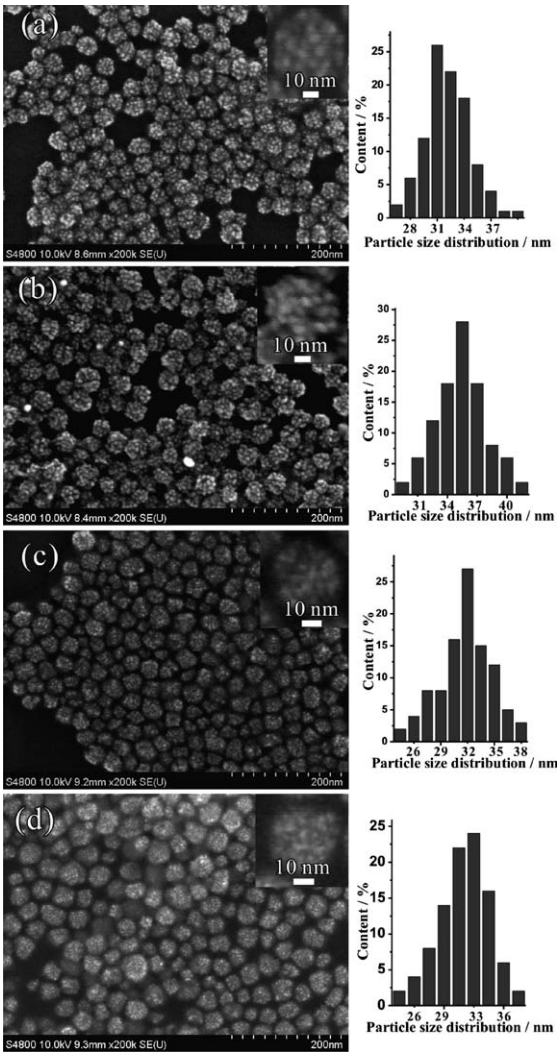

Fig. 1 Typical SEM images and size distribution histograms of as-prepared (a) porous palladium nanospheres, (b) porous Pd_3Ag_1 nanospheres, (c) porous Pd_3Pt_1 nanospheres and (d) porous $Pd_3Pt_{0.5}Ag_{0.5}$ nanospheres. The insets in (a–d) are high magnification SEM images of single nanospheres.

assembled from nanoparticles with a size in the range of 6–10 nm. And the Pd_3Pt_1 and $Pd_3Pt_{0.5}Ag_{0.5}$ nanospheres also have similar hierarchical structures with nanorods as the primary building blocks.

The structure and phase analysis of the as-prepared nanospheres were performed by XRD. Fig. 3 shows the XRD patterns of the Pd nanospheres, Pd–Pt nanospheres, Pd–Ag nanospheres and Pd–Pt–Ag nanospheres. All of these XRD patterns can be indexed as the face-centred cubic (fcc) phase. For the Pd nanospheres (Fig. 3a), the lattice parameter a was calculated to be 0.3890(1) by the least-squares method, which matched the fcc crystalline Pd structure (JCPDS number: 46-1043) very well. For the Pd based alloys, as shown in Fig. 3b–3g, the diffraction peaks deviate from that of pure Pd, which is obviously caused by the lattice expansion when Pt and/or Ag atoms are alloyed into the crystal lattice due to that the atom radii of Ag (0.144 nm) and Pt (0.139 nm) being larger than that of Pd (0.137 nm). According to

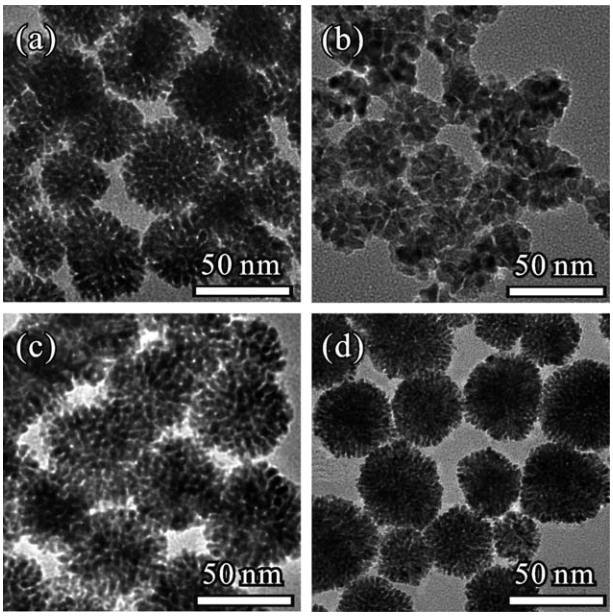

Fig. 2 Typical TEM images of the as-prepared (a) porous palladium nanospheres, (b) porous Pd_3Ag_1 nanospheres, (c) porous Pd_3Pt_1 nanospheres and (d) porous $Pd_3Pt_{0.5}Ag_{0.5}$ nanospheres.

the positions of the diffraction peaks, the lattice parameters were calculated by the least-squares method as listed in Table 1. In this table, the compositions of the binary alloys were evaluated by supposing that the crystal cell parameter linearly depends on the composition of alloy metals, which agrees well with the molar ratio of precursors fed into the reaction. These results indicate that composition of these nanospheres can be easily adjusted by controlling the molar ratio of the precursors.

The broad diffraction peaks suggest that the as-prepared nanospheres consist of small nanocrystallites. The average crystallite size of the Pd primary nanoparticles was 6.9 nm calculated from the peak width of the (111) diffraction according to the Scherrer's equation. Similarly, the average crystallite size

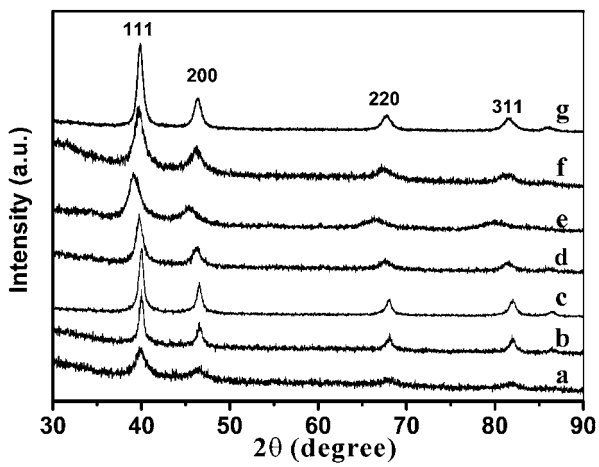

Fig. 3 XRD patterns of the as-synthesized (a) Pd nanospheres, (b) $Pd_3Pt_{0.5}$ nanospheres, (c) Pd_3Pt_1 nanospheres, (d) $Pd_3Ag_{0.5}$ nanospheres, (e) Pd_3Ag_1 nanospheres, (f) $Pd_3Pt_1Ag_1$ nanospheres, and (g) $Pd_3Pt_{0.5}Ag_{0.5}$ nanospheres.

Table 1 The lattice parameters, particle size and composition of the as-prepared nanospheres

	Particle size (nm)	Primary particle size (nm)	Cell parameter *a* (nm)	Evaluated atomic ratio of Pd
bulk Pd			0.38902	
bulk Pt			0.39231	
bulk Ag			0.40861	
Pd nanospheres	25–40	6.9	0.3890(1)	
Pd_3Pt_1	30–50	11.8	0.3899(1)	73%
$Pd_3Pt_{0.5}$	30–50	9.4	0.3896(1)	85%
Pd_3Ag_1	25–40	5.9	0.3959(3)	65%
$Pd_3Ag_{0.5}$	25–40	9.1	0.3918(2)	86%
$Pd_3Pt_1Ag_1$	25–40	6.9	0.3923(2)	—
$Pd_3Pt_{0.5}Ag_{0.5}$	25–40	11.3	0.3913(1)	—

of the primary building nanocrystallites of Pd based alloy nanospheres were calculated and listed in Table 1. It should be pointed out that some of the average sizes were a little bigger than that measured from the TEM images, which could be due to the oriented attachment of the primary crystallites in the hierarchical nanospheres.

CV measurement of the porous nanospheres

The electrochemical catalytic activity of the as-prepared nanospheres for the oxidation of formic acid was studied using cyclic voltammetry in 0.50 mol L^{-1} H_2SO_4 + 0.50 mol L^{-1} HCOOH electrolyte at a scan rate of 50 mV s^{-1}. The electrochemical reactivity and electrochemically active surface area of different catalysts were determined by the area of the hydrogen adsorption/desorption peaks in the CV measurements performed in 0.50 mol L^{-1} H_2SO_4 electrolyte at a scan rate of 50 mV s^{-1}. As it is well known, in direct methanol oxidation fuel cells, CO intermediates would be produced, which further poison the catalysts. To study the ability to tolerate CO, the electrochemical behaviour of the catalysts were also measured in an N_2-purged 0.10 mol L^{-1} $HClO_4$ + 0.10 mol L^{-1} CH_3OH solution. By comparing the hydrogen adsorption/desorption peaks in the presence of CH_3OH with those in the absence of CH_3OH, the CO tolerance abilities were tested.[29]

Fig. 4a is the CV curves of Pd nanospheres and Pd–Pt alloy nanospheres in the 0.50 mol L^{-1} H_2SO_4 + 0.50 mol L^{-1} HCOOH aqueous solution. The peak potential of the formic acid oxidation for the as-prepared Pd nanosphere catalyst electrode is about 0.49 V and the corresponding peak current density is 2.27 mA cm^{-2}. When the Pt was alloyed into the Pd nanospheres, the onset oxidation potential obviously shifted negatively, and the corresponding current density greatly increased. The corresponding peak current densities increase to 2.8 mA cm^{-2}, and 4.4 mA cm^{-2} for the $Pd_3Pt_{0.5}$ and Pd_3Pt_1 alloy nanosphere electrodes, respectively. These results indicated that the alloying of platinum into Pd nanospheres can improve the catalytic activity of formic acid oxidation. It has been known that the catalytic activity of Pt for the formic acid oxidation is much larger than that of Pd. The alloying of Pt into Pd therefore improves the catalytic activity, due to the presence of Pt atoms on nanoparticle surfaces.[22] However, it is also known that platinum catalysts are easily poisoned by CO, which can be produced during the oxidation of organic fuels.[21,29–32] Therefore, the ability of CO tolerance for the as-prepared Pd–Pt alloy catalysts should be taken into account. As shown in Fig. 4b, the electrochemical active surface area of the Pd_3Pt_1 alloy nanosphere electrode obviously decreased in the 0.10 mol L^{-1} $HClO_4$ + 0.10 mol L^{-1} CH_3OH solution by evaluating the hydrogen adsorption/desorption peak area compared to the CVs obtained from the 0.10 mol L^{-1} $HClO_4$ solution. When the Pt content in the Pd–Pt alloy reached 14% and 25% (atomic percentage), the electrochemical active surface area respectively reduce to 57.2% and 34.6% when measured in the 0.10 mol L^{-1} $HClO_4$ + 0.10 mol L^{-1} CH_3OH solution (Table 2). As a result, with Pt alloying of the Pd nanospheres, although the catalytic activity increases, the CO tolerance seriously decreases.

Fig. 4c is the CVs of Pd nanosphere and Pd–Ag alloy nanosphere electrodes in the 0.50 mol L^{-1} H_2SO_4 + 0.50 mol L^{-1} HCOOH aqueous solution. The peak potential for the formic

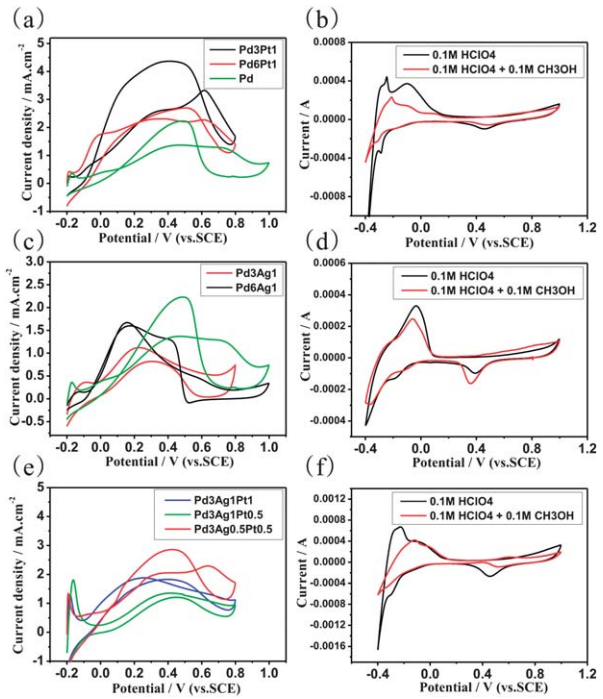

Fig. 4 (a, c, e) CV traces of Pd and its alloys in 0.50 mol L^{-1} H_2SO_4 + 0.50 mol L^{-1} HCOOH aqueous solution; (b, d, f) CV curves of Pd_3Pt_1, Pd_3Ag_1, $Pd_3Pt_{0.5}Ag_{0.5}$ in an N_2-purged 0.10 mol L^{-1} $HClO_4$ solution with (red) and without (black) 0.10 mol L^{-1} methanol. Scan rate: 50 mV s^{-1}.

Table 2 Integral charges (Q) of hydrogen desorption of the as-prepared nanospheres in $HClO_4$ with or without CH_3OH

	Pd	$Pd_3Pt_{0.5}$	Pd_3Pt_1	$Pd_3Ag_{0.5}$	Pd_3Ag_1	$Pd_3Pt_1Ag_1$	$Pd_3\ Pt_{0.5}Ag_{0.5}$
Q without CH_3OH (C)	1.021×10^{-3}	1.675×10^{-3}	2.348×10^{-3}	1.335×10^{-3}	3.245×10^{-4}	2.315×10^{-3}	2.589×10^{-3}
Q with CH_3OH (C)	7.047×10^{-4}	9.585×10^{-4}	8.126×10^{-4}	9.893×10^{-4}	2.817×10^{-4}	1.628×10^{-3}	1.775×10^{-3}
Q (with CH_3OH)/Q (without CH_3OH)	69.0%	57.2%	34.6%	74.1%	86.8%	70.3%	68.6%

acid oxidation for the $Pd_3Ag_{0.5}$ catalyst electrode is at 0.26 V and the corresponding peak current density is 1.73 mA cm^{-2}. With the amount of silver increasing, the corresponding peak current densities decrease. However, the peak potentials are obviously negatively shifted with the increasing content of Ag. Moreover, it can be observed from Fig. 4d that when Ag was alloyed into the Pd nanostructures, the electrochemical active surface area for the hydrogen adsorption/desorption peaks in the 0.10 mol L^{-1} $HClO_4$ + 0.10 mol L^{-1} CH_3OH solution only slightly reduced in comparison to that in the 0.10 mol L^{-1} $HClO_4$ solution. This result indicates that the alloying of Ag into Pd nanostructures leads to very excellent CO tolerance ability. It could be observed in the present case that when the Ag content increased from 14% to 25% (atomic percentage), the electrochemical active surface area in the presence of CH_3OH may increase from 74.1% to 86.8%, and both of them were larger than that of the as prepared Pd porous nanospheres. A similar phenomenon was also observed for PtAg nanotubes for formic acid oxidation[32] and Pd–Ag/C catalysts towards methanol oxidation in alkaline media.[33] According to the bi-functional mechanism, after the combining Ag with Pd, the Ag may activate water at lower potentials than Pd and the activated water can oxidize the adsorbed CO and therefore liberate Pd active sites.[33] With the Ag content increased, the oxidative removal of CO is further facilitated at the PdAg nanospheres and the ability of CO tolerance of the catalysts has been improved.

The above electrochemical catalytic properties of Pd–Pt and Pd–Ag porous nanospheres suggested that by alloying with suitable metals and adjusting the composition of the alloy nanospheres, the performance of Pd based catalysts could be optimized. Directed by the strategy, ternary Pd–Pt–Ag alloy nanospheres were synthesized and their electrochemical catalytic properties for formic acid oxidation are shown in Fig. 4e. It can be observed that with the increase of silver content in Pd–Ag–Pt alloy nanospheres, the corresponding peak current density decrease, while an increase in the content of Pt would have the opposite efect. By adjusting the molar ratio of Pd, Pt and Ag in the Pd–Pt–Ag alloy nanospheres, the oxidation potential of the formic acid as well as the corresponding peak current density can be optimized. It was found that the peak potential and current of the $Pd_3Pt_{0.5}Ag_{0.5}$ catalyst electrode is 0.42 V and 2.93 mA cm^{-2}, respectively, which are superior to that of the as prepared Pd nanospheres. Furthermore, the CO tolerance is comparable to that of the as prepared Pd nanospheres (see Fig. 4f and Table 2).

Conclusions

In summary, Pd porous nanospheres as well as Pd–Pt, Pd–Ag and Pd–Pt–Ag alloy nanospheres have been successfully prepared through a facile aqueous solution process. These nanospheres were assembled from small nanoparticle building blocks. The composition of these alloy nanospheres can be easily adjusted by controlling the molar ratio of the precursors. Electrochemical measurements indicated that the electrocatalytic activities of these alloy nanospheres towards formic acid oxidation depended on the composition of the nanospheres. By judicious selection of doping metal and adjusting the composition of the Pd based alloy nanospheres, the performance of the Pd based catalysts for formic acid oxidation could be optimized. It is reasonable to believe that the mentioned strategy could be extended to prepare other metal based catalysts.

Acknowledgements

This work was supported by the National Natural Science Foundation of China (Grant Nos. 20725310, 21021061 and 21073145), Key Scientific Project of Fujian Province of China (Grant No. 2009HZ0002-1), the National Basic Research Program of China (Grant Nos. 2007CB815303, 2009CB939804) and NCET in Fujian Province University.

References

1 A. S. Aricò, P. Bruce, B. Scrosati, J. M. Tarascon and W. V. Schalkwijk, *Nat. Mater.*, 2005, **4**, 366.
2 U. B. Demirci, *J. Power Sources*, 2007, **169**, 239.
3 C. Rice, S. Ha, R. I. Masel, P. Waszczuk, A. Wieckowsk and T. Barnard, *J. Power Sources*, 2002, **111**, 83.
4 C. Rice, S. Ha, R. I. Masel and A. Wieckowski, *J. Power Sources*, 2003, **115**, 229.
5 X. W. Yu and P. G. Pickup, *J. Power Sources*, 2008, **182**, 124.
6 R. F. Wang, S. J. Liao and S. Ji, *J. Power Sources*, 2008, **180**, 205.
7 W. J. Zhou, Z. H. Zhou, S. Q. Song, W. Z. Li, G. Q. Sun, P. Tsiakaras and Q. Xin, *Appl. Catal., B*, 2003, **46**, 273.
8 T. J. Schmidt, U. A. Paulus, H. A. Gasteiger and R. J. Behm, *J. Electroanal. Chem.*, 2001, **508**, 41.
9 E. Antolini, *Energy Environ. Sci.*, 2009, **2**, 915.
10 V. Mazumder, Y. M. Lee and S. H. Sun, *Adv. Funct. Mater.*, 2010, **20**, 1224.
11 R. Larsen, S. Ha, J. Zakzeski and R. I. Masel, *J. Power Sources*, 2006, **157**, 78.
12 Z. Y. Bai, L. Yang, L. Li, J. Lv, K. Wang and J. Zhang, *J. Phys. Chem. C*, 2009, **113**, 10568.
13 J. J. Ge, W. Xing, X. Z. Xue, C. P. Liu, T. H. Lu and J. H. Liao, *J. Phys. Chem. C*, 2007, **111**, 17305.
14 V. Mazumder and S. H. Sun, *J. Am. Chem. Soc.*, 2009, **131**, 4588.
15 S. Y. Wang, X. Wang and S. P. Jiang, *Nanotechnology*, 2008, **19**, 455602.
16 X. G. Wang, W. M. Wang, Z. Qi, C. C. Zhao, H. Ji and Z. H. Zhang, *Electrochem. Commun.*, 2009, **11**, 1896.
17 Z. Yin, H. J. Zheng, D. Ma and X. H. Bao, *J. Phys. Chem. C*, 2009, **113**, 1001.
18 M. S. Bakshi, *J. Phys. Chem. C*, 2009, **113**, 10921.
19 B. Lim, M. Jiang, P. H. Camargo, E. C. Cho, J. Tao, X. Lu, Y. Zhu and Y. Xia, *Science*, 2009, **324**, 1302.
20 Z. M. Peng and H. Yang, *J. Am. Chem. Soc.*, 2009, **131**, 7542.
21 H. Lee, S. E. Habas, G. A. Somorjai and P. D. Yang, *J. Am. Chem. Soc.*, 2008, **130**, 5406.
22 X. Q. Huang, H. H. Zhang, C. Y. Guo, Z. Y. Zhou and N. F. Zheng, *Angew. Chem., Int. Ed.*, 2009, **48**, 4808.
23 Q. Yuan, Z. Y. Zhou, J. Zhuang and X. Wang, *Chem. Commun.*, 2010, **46**, 1491.

24 Q. F. Yi, W. Huang, X. P. Liu, G. R. Xu, Z. H. Zhou and A. C. Chen, *J. Electroanal. Chem.*, 2008, **619–620**, 197.
25 S. J. Guo, S. J. Dong and E. K. Wang, *ACS Nano*, 2010, **4**, 547.
26 N. Tian, Z. Y. Zhou and S. G. Sun, *Chem. Commun.*, 2009, 1502.
27 Z. Y. Zhou, N. Tian, Z. Z. Huang, D. J. Chen and S. G. Sun, *Faraday Discuss.*, 2009, **140**, 81.
28 J. Watt, S. Cheong, M. F. Toney, B. Ingham, J. Cookson, P. T. Bishop and R. D. Tilley, *ACS Nano*, 2010, **4**, 396.
29 C. X. Xu, Y. Zhang, L. Q. Wang, L. Q. Xu, X. F. Bian, H. Y. Ma and Y. Ding, *Chem. Mater.*, 2009, **21**, 3110.
30 H. Q. Li, Q. Xin, W. Z. Li, Z. H. Zhou, L. H. Jiang, S. H. Yang and G. Q. Sun, *Chem. Commun.*, 2004, 2776.
31 Q. J. Xu, X. J. Zhou, Q. X. Li, J. G. Li and Y. Z. Zhao, *Adv. Mater. Res.*, 2010, **152–153**, 1620.
32 Y. Z. Lu and W. Chen, *J. Phys. Chem. C*, 2010, **114**, 21190.
33 Y. Wang, Z. M. Sheng, H. B. Yang, S. P. Jiang and C. M. Li, *Int. J. Hydrogen Energy*, 2010, **35**, 10087.